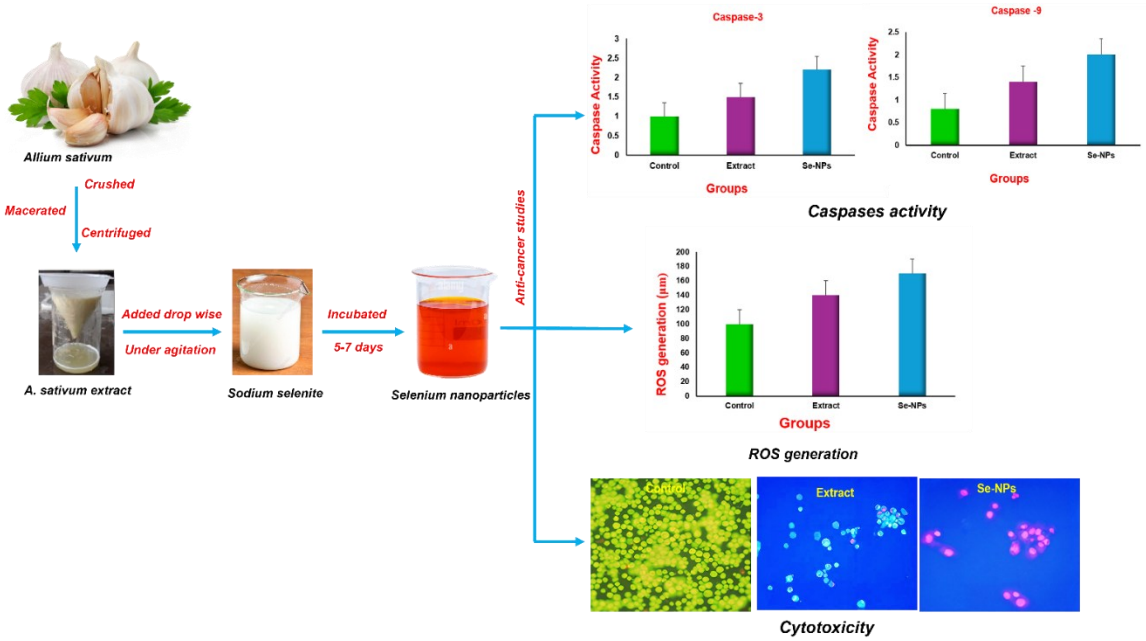
Green Synthesis of Selenium Nanoparticles Using *Allium sativum* Extract: *In-vitro* Evaluation of their Anticancer Potential against Breast Carcinoma

Fengqi Chen,[#] Qi Han,[#] and Lan Yang *

Corresponding author: 15172506591@163.com

DOI: 10.15376/biores.21.3.8015-8030

GRAPHICAL ABSTRACT



Green Synthesis of Selenium Nanoparticles Using *Allium sativum* Extract: *In-vitro* Evaluation of their Anticancer Potential against Breast Carcinoma

Fengqi Chen,[#] Qi Han,[#] and Lan Yang *

A green synthesis approach was implemented to establish an economical and environmentally favorable protocol to produce selenium nanoparticles (Se-NPs) by utilizing aqueous extract from *Allium sativum.* The Se-NPs were characterized using a combination of spectroscopic and microscopic techniques. The anticancer efficacy of Se-NPs was assessed using MCF-7 cell line and it demonstrated concentration-dependent suppression of MCF-7 cell proliferation. The activation of caspases by Se-NP treatment was further demonstrated by fluorescence microscopy, which resulted in the development of typical apoptotic features, including nuclear condensation and cell membrane blebbing. Furthermore, the Se-NP exposure was linked to increased reactive oxygen species (ROS), suggesting that oxidative stress is a critical mediator of apoptosis in MCF-7 cells. Overall, the results indicate that Se-NPs can act as a selective anticancer drug and induce apoptosis through ROS-mediated pathways. These findings lend credence to the ability of green synthesized Se-NPs as a novel nanotherapeutic platform for cancer treatment.

DOI: 10.15376/biores.21.3.8015-8030

Keywords: Selenium nanoparticles; Allium sativum; Cell viability; Anti-cancer; Breast cancer; Caspases; ROS

*Contact information: Department of Thyroid and Breast Surgery, Zhongnan Hospital of Wuhan University, Wuhan, 430000, Hubei, China; [#] Co-first authors; * Corresponding author: 15172506591@163.com*

INTRODUCTION

Globally, cancer is the most prevalent cause of mortality, with around ten million new cases diagnosed each year, resulting in over six million fatalities (Haggar *et al*. 2009). One of the most prevalent malignancies among women worldwide is breast cancer, with its incidence consistently rising over time (Kotepui 2016). The disease severely impacts morbidity and mortality, especially in people from the United States, Northwestern Europe, and South Korea, and its prevalence is increasing (Leong *et al*. 2010). Conventional cancer treatments, primarily chemotherapy and radiotherapy, remain the standard approach, despite extensive research efforts. Nevertheless, these treatments are accompanied by substantial drawbacks, particularly their lack of selectivity, which frequently results in the elimination of both healthy and malignant cells (Da-Yong *et al*. 2013). Standard therapeutic measures, including surgery, chemotherapy, and radiation, often lead to side consequences such as bone marrow suppression, thrombocytopenia, and gastrointestinal issues (Muller *et al*. 2000; Alyamkina *et al*. 2010). These problems have stimulated increasing interest in the investigation of alternate treatment options.

A promising strategy entails the utilization of nanotechnology-based therapies (Park *et al*. 2008; Ma *et al*. 2024; Azimizonuzi *et al*. 2025). Metal nanoparticles (MNPs)

produced from proteins obtained from natural sources have garnered interest because of their unique physicochemical features. Selenium (Se) is an essential micronutrient and serves as an important cofactor in several antioxidant enzymes (Srivastava and Mukhopadhyay 2013; Husen and Siddiqi 2014). Recently, selenium nanoparticles (Se-NPs) have attracted significant interest owing to their remarkable antibacterial and anticancer attributes, positioning them as prospective candidates for nanomedicine applications (Forootanfar *et al.* 2013; Wadhwani *et al*. 2016). A significant benefit of Se-NPs is their relatively reduced toxicity compared to inorganic and organic selenium alternatives (Shakibaie *et al*. 2010), highlighting the necessity of refining their production methods. Patil and Kim (2018) have conducted thorough research on the synthesis of MNPs utilizing marine microorganisms for biological applications.

Se-NPs can be produced using various chemical and physical methods (Shehata *et al*. 2023; Iranifam *et al*. 2013). Conventional methods frequently utilize hazardous chemicals and produce environmentally detrimental byproducts, rendering them both expensive and less sustainable (Alsammarraie *et al*. 2018). Biological or green synthetic technologies provide numerous advantages, such as environmental sustainability, economic efficiency, and biocompatibility. These methods frequently produce very stable Se-NPs, usually capped with biomolecules such as proteins, which inhibit agglomeration and augment biological activity (Shedbalkar *et al*. 2014; Singh *et al*. 2015). Selenium nanoballs measuring 3 to 18 nm were effectively produced utilizing *Vitis vinifera* extracts (Sharma *et al*. 2014). Li *et al*. (2007) similarly documented the production of selenium nanorods and nanospheres utilizing *Capsicum annuum* extracts. Colloidal Se-NPs generated from *Terminalia arjuna* indicated potential anticancer action against human breast cancer cells (Prasad *et al*. 2014), whereas oval-shaped Se-NPs made from fenugreek seed extract also had promising anticancer properties (Ramamurthy *et al*. 2013).

In this study, Se-NPs were produced by utilizing *Allium sativum (A. sativum)* extract. Since antiquity, *A. sativum,* a member of the Liliaceae family, which is commonly known as garlic, has been cherished for its extensive array of therapeutic properties. Its bioactive compounds have exhibited a diverse range of pharmacological effects, such as antimicrobial (Ankri and Mirelman 1999), antihypertensive (Nwokocha *et al*. 2011), antihyperlipidemic (Gupta and Porter 2001), antidiabetic (Liu *et al*. 2007), anticancer (Tsubura *et al*. 2011), cardioprotective (Dennis 2021), neuroprotective (Vinaykumar 2003), antithrombotic, and anti-platelet aggregation activities (Liao *et al*. 2000). Furthermore, *A. sativum* has demonstrated efficacy in the treatment of arthritic conditions and allergic responses. The therapeutic potential of Se-NPs synthesised using *A. sativum* extract may be improved by the presence of a variety of bioactive phytochemicals that naturally occur in the plant. *A. sativum* is known as a significant source of pharmacological significant metabolites, including sulfur-containing compounds, flavonoids, and phenolics, which exhibit antioxidants, antimicrobial, anti-inflammatory, and anticancer properties. The incorporation of these biomolecules during nanoparticle synthesis may enhance the biological efficacy and stability of the resulting Se-NPs. Consequently, *A. sativum* -mediated Se-NPs are a promising nanoplatform that has the potential to be used in a variety of biomedical and therapeutic applications.

The novelty of this study lies in the use of *Allium sativum* extract, a bioresource rich in sulfur-containing compounds and diverse pharmacologically active metabolites, to synthesize Se-NPs *via* a simple, inexpensive aqueous green route. Unlike previous reports employing *Vitis vinifera*, *Capsicum annuum*, *Terminalia arjuna*, or fenugreek extracts, the present work demonstrates that garlic-mediated Se-NPs not only exhibit uniform

morphology and colloidal stability but also can induce apoptosis in Michigan Cancer Foundation-7 (MCF-7) cells through a clearly defined mechanism involving ROS generation and caspase-3/9 activation. This mechanistic insight, combined with the eco-friendly synthesis approach, highlights the distinct biomedical potential of *A. sativum*-derived Se-NPs as promising candidates for targeted breast cancer therapy.

In this study Se-NPs were effectively synthesized using an inexpensive aqueous extract of *A. sativum*, utilizing a green synthetic approach. To highlight their biomedical relevance, the anticancer efficacy of Se-NPs was tested on the MCF-7 human breast cancer cell line.

MATERIALS AND METHODS

Preparation of Extract

Fresh *A. sativum* cloves (5 g) were collected, thoroughly washed with distilled water, and the outer membrane was removed. Using Mortar and pestle the cloves were delicately crushed. Macerate the crushed material in 30 mL of Tris–Cl buffer, adjusted to a pH of 7.5. and then centrifuged at 10,000 rpm for 10 min at 4 °C. The resulting supernatant was collected and transferred to a sterile centrifuge tube, where it was stored under refrigeration for later use.

Synthesis of Se-NPs

Under constant magnetic agitation, 2 mL of the *A. sativum* extract was added dropwise to 30 mL of a 10 mM sodium selenite solution. Incubate the mixture on a thermo-orbital agitator at 120 rpm for a period of 5 to 7 days, while being maintained in light conditions at 36 °C. The absorption spectra were recorded using UV–Visible spectroscopy to monitor the progress of selenium ion reduction and nanoparticle formation on a periodic basis (Prasad and Selvaraj 2014).

Characterization

The optical properties of the Se-NPs were analyzed using a UV–Visible spectrophotometer within the wavelength range of 200 to 700 nm using a PerkinElmer Lambda 25 spectrometer (Shanghai, China). Transmission Electron Microscopy (TEM) was utilized to determine their size and morphology using a FEI Titan (from FEI Company, Shanghai, China). Phase purity and crystallinity were examined through X-ray diffraction (XRD) employing Cu Kα radiation A MAXima XRD-7000 system (Sigma-Aldrich, Shanghai, China). Functional groups involved in the formation and stabilization of the nanoparticles were identified *via* Fourier transform infra-red (FTIR) spectroscopy using a PerkinElmer Spectrum 2 FT-IR spectrometer. Additionally, the mean particle size and zeta potential of the Se-NPs were assessed using a dynamic light scattering (DLS) particle size analyser using a Brookhaven Zeta-PAL zeta potential analyser (Shanghai, China)

Anti-cancer Studies

Cell culture

MCF-7 cell lines were cultured in 75-cm² cell culture containers and maintained under humidified conditions (at 37 °C, 5 % CO_2). Eagle's minimum essential medium was used to cultivate MCF-7 cells. Upon attaining approximately 80 % confluence, cell lines were trypsinized and subsequently seeded into 96-well and 24-well plates for subsequent

experiments. The cells were exposed to different concentrations of Se-NPs after 24 h of incubation to facilitate cell attachment.

MTT Assay

To assess the viability of cells after Se-NPs treatment, a modified variant of the MTT assay protocol (Stockert *et al*. 2012) was implemented. To facilitate adherence, the MCF-7 was distributed in 96-well plates and incubated for 24 h under standard conditions. Then the cells were exposed to different concentrations of Se-NPs for an additional 24 h. To facilitate the formation of insoluble formazan crystals within metabolically active cells, 10 µL of MTT solution was added to each well following the treatment. The plates were then incubated at 37 °C for 4 h. The formazan was dissolved in each well by adding 100 µL of DMSO after incubation. The absorbance at 570 nm was measured using a microplate reader, and the cell viability was determined in relation to the untreated controls.

Acridine orange/ethidium bromide staining

To evaluate apoptosis in MCF-7 cells treated with Se-NP, acridine orange/ethidium bromide (AO/EB) dual fluorescence staining was implemented, as per a technique that was previously described with minor modifications (Kasibhatla *et al*. 2006). To facilitate cell attachment, MCF-7 cells were distributed into six-well plates and incubated for 24 h. Subsequently, treat the cells with Se-NPs. The control group consisted of cells that were not treated. In PBS, a staining solution was generated by combining equal volumes of AO and EB, each at a concentration of 100 µg/mL. About 20 µL of the dye mixture was added to both the treated and control cells following the treatment. The fluorescence intensity was measured using fluorescence microscope. This assay enabled the visualization of Se-NP induced apoptotic alterations to distinguish between viable (green), early apoptotic (bright green with condensed nuclei), and late apoptotic or necrotic (orange to red) cells.

Determination of ROS

The 2′,7′-dichlorodihydrofluorescein diacetate (DCFH-DA) assay was employed to evaluate intracellular ROS levels, as previously described (Shim *et al*. 2007). Under conventional culture conditions, the MCF-7 cells were seeded into 24-well plates and incubated for 24 h. Phosphate-buffered saline (PBS) was used to cleanse the cells twice after incubation. The cells were exposed to biosynthesized Se-NPs for 24 h. Then incubated the cells with 20 µM DCFH-DA for 30 min at 37 °C to detect ROS. The fluorescent compound 2′,7′-dichlorofluorescein (DCF) is produced by the intracellular hydrolysis of the non-fluorescent DCFH-DA and the subsequent oxidation by ROS. Cells were cleansed with PBS following staining, and 2 mL of PBS was added. The fluorescence intensity was measured using spectrofluorometer.

Evaluation of caspase activities

The activities of caspase-3 and caspase-9 were quantified using commercially available luminescent assay kits, following the manufacturer's instructions. In a nutshell, MCF-7 cells were introduced in a 96-well plate and incubated for 24 h (37 °C, 5 % CO_2). The plates were equilibrated to room temperature following treatment with Se-NPs and the application of appropriate controls. Subsequently, 100 µL of Caspase-Glo® 3 or Caspase-Glo® 9 reagent was added to each well containing 100 µL of culture medium. The plate was then covered and gently agitated at 500 rpm for 30 s to ensure thorough interaction between the reagent and the cells. Following a 30-min incubation at room temperature,

luminescence was measured at an optical density of 405 nm using a microplate reader. In Se-NPs treated cells, caspase activation was employed as a marker for apoptosis induction.

RESULTS AND DISCUSSION

Characterization

UV–Visible spectrophotometric analysis

The formation of Se-NPs was visually evidenced by a color change in the Na_2SeO_3 solution upon the addition of *A. sativum* extract, signifying the reduction of selenite ions to elemental selenium. The transition of the reaction mixture from colorless to brick red confirmed the successful synthesis of Se-NPs. Prolonged incubation for an additional two days slightly intensified the red coloration. This characteristic red hue, attributed to the excitation of surface plasmon resonance (SPR), a distinctive property of Se-NPs indicated the effective formation of the nanoparticles. Further confirmation of elemental Se-NPs was achieved through UV–Visible spectrophotometric analysis, showing an absorbance maximum at 280 nm within the 200 to 700 nm range (Fig. 1).

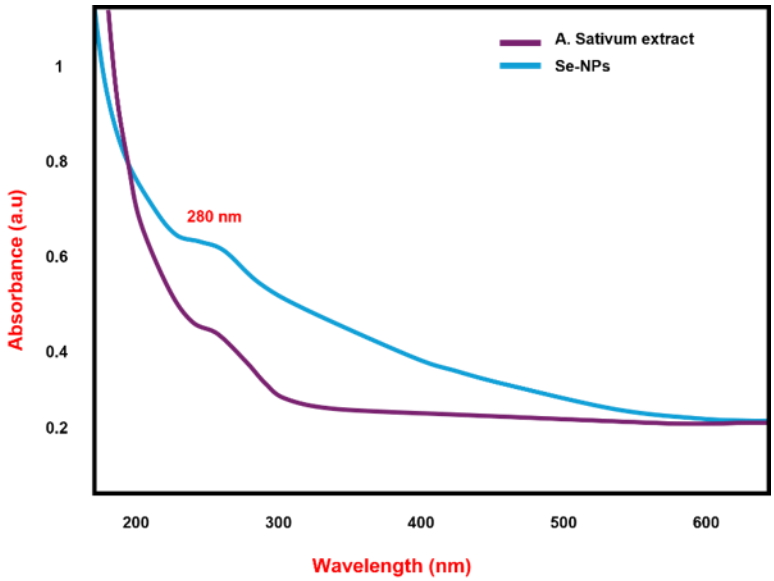


Fig. 1. UV-Visible spectra of synthesized Se-NPs and *A. sativum* extract. Se-NPs confirmed by SPR peak at 280 nm, indicating successful reduction of selenite to elemental selenium

FTIR

FTIR results are illustrated in Fig. 2. The absorbance peak underwent a significant shift from 3274 cm^{-1} to 3382 cm^{-1}, indicating the involvement of hydroxyl and amino functional groups during the formation of Se-NPs. Additional shifts were observed at a variety of spectral positions, including the peak at 2890 cm^{-1}, which was shifted to 2888 cm^{-1} (C–H), the peak at 1632 cm^{-1}, which was shifted to 1642 cm^{-1} (C=C), the peak at 1405 cm^{-1}, which was shifted to 1415 cm^{-1}, (N–O), and the peak at 1012 cm^{-1} was shifted to 1020 cm^{-1} (C–O). These spectral shifts indicate that sodium selenite interacted with *A. sativum* extract metabolites during the formation of nanoparticles. Furthermore, the *A. sativum* extract and the synthesized Se-NPs exhibited a medium-intensity peak at 705 cm^{-1} (C–H). The FTIR spectra further indicated that the nitro ($–NO_2$) and carboxyl (–COOH)

groups present in the *A. sativum* extract played a substantial role in the reduction and stabilization of Se-NPs.

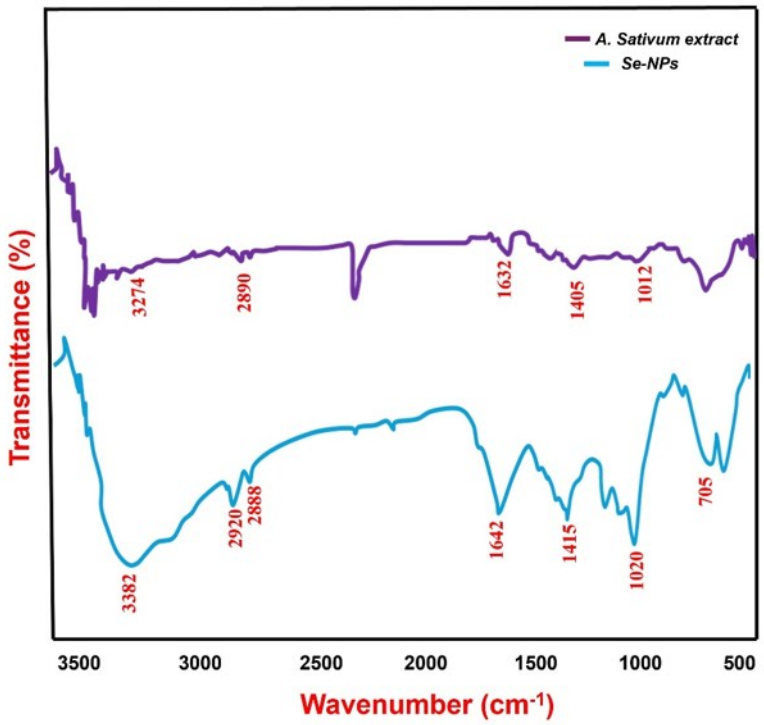


Fig. 2. FTIR spectra of synthesized Se-NPs and *A. sativum* extract showing characteristic functional group vibrations

TEM

The morphology and size distribution of the Se-NPs were analyzed using TEM. Based on the TEM images (Fig. 3), the nanoparticles were uniformly distributed, monodispersed, and predominantly spherical, with size ranges from 40 to 100 nm under the specified synthesis conditions.

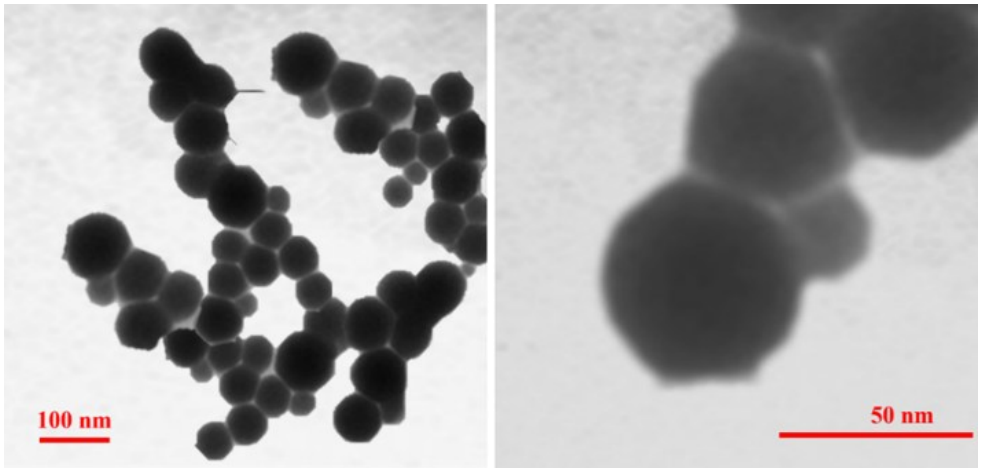


Fig. 3. TEM images of Se-NPs synthesized using *A. sativum* extract at magnifications of 50 nm and 10 nm

Selected area electron diffraction (SAED)

The crystalline nature of the synthesized Se-NPs was verified by the SAED pattern. The (100), (101), (110), and (102) lattice planes of crystalline selenium were identified as distinct diffraction rings (Fig. 4). The effective formation of Se-NPs under the applied synthesis conditions is further supported by the well-defined crystalline structure indicated by these reflections.

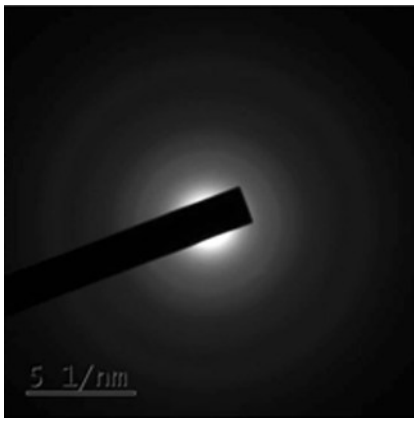


Fig. 4. SAED pattern of Se-NPs synthesized using *A. sativum* extract

XRD

The crystallinity of the Se-NPs was verified by the eight distinct peaks present in the XRD pattern. The 2θ values at 23.59°, 29.78°, 41.29°, 43.67°, 45.84°, 51.74°, 56.13°, and 62.81° were indicative of the (100), (101), (110), (102), (111), (201), (112), and (202) crystal planes of hexagonal selenium, respectively. The crystalline phase and structural identity of the fabricated Se-NPs were further validated by the fact that these diffraction peaks are in strong agreement with the standard data (JCPDS file no. 06-0362) (Fig. 5).

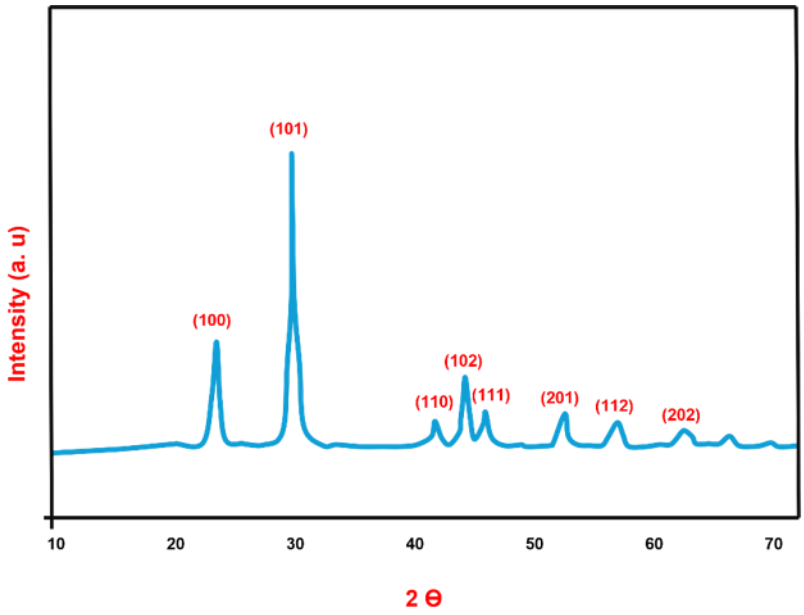


Fig. 5. XRD pattern of Se-NPs synthesized using *A. sativum* extract and the abscissa is labeled as 2θ (°) and the ordinate as intensity (a.u.)

EDX

Figure 6 illustrates the EDX spectrum used to confirm the elemental composition of the Se-NPs. The successful incorporation of elemental selenium was indicated by the observation of a prominent signal. Carbon, oxygen, and sodium peaks were also detected in addition to selenium, which are likely the result of residual precursor compounds, and the *A. sativum* extract used in the synthesis process. As illustrated in Fig. 6, selenium comprised the preponderance of the elemental composition, accounting for approximately 82 %. Other elements of carbon (5 %), oxygen (6 %), and sodium (4 %) were also found.

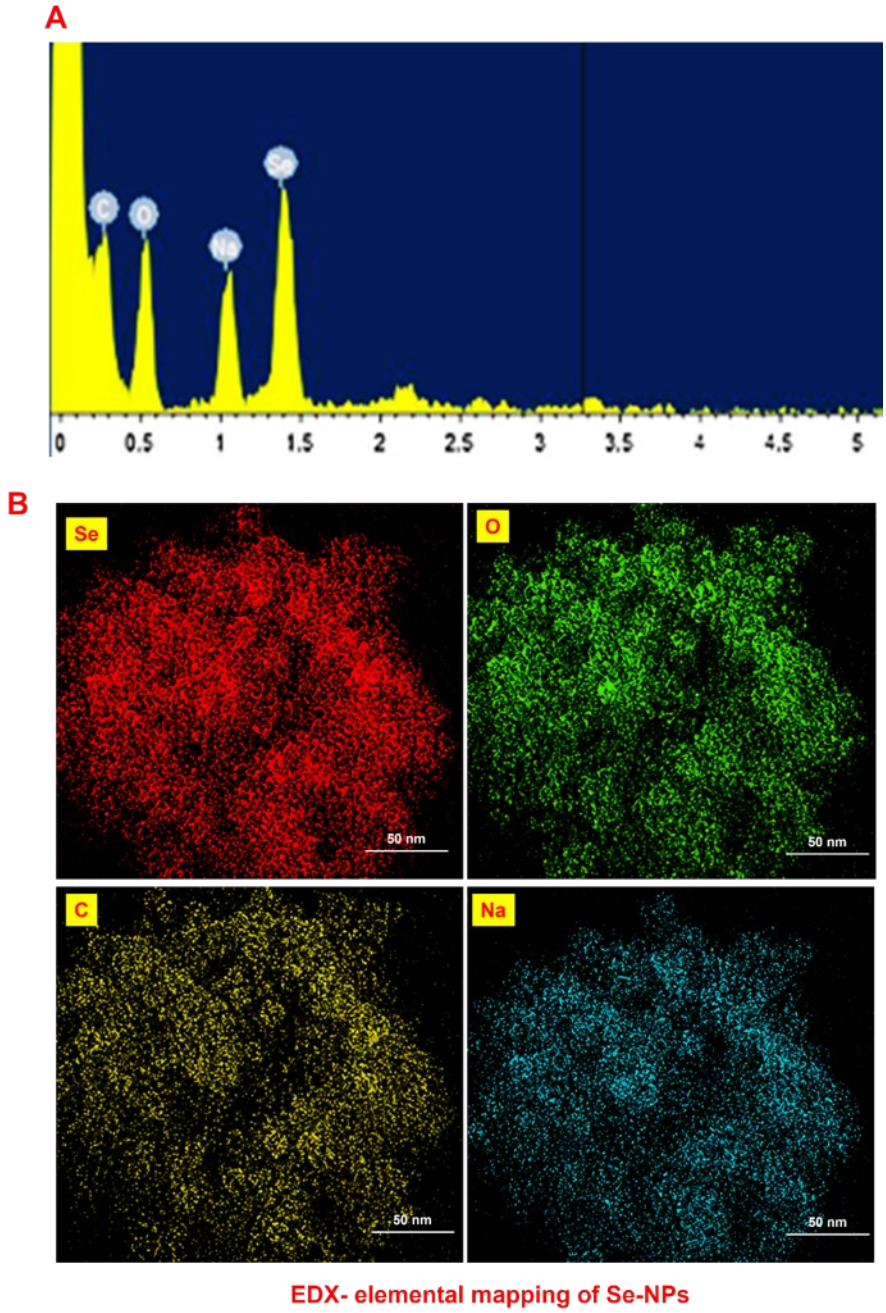


Fig. 6. (A) EDX spectrum of Se-NPs synthesized using *A. sativum* extract showing characteristic peaks of C, O, Na, and Se. **(B)** Elemental mapping of Se-NPs

DLS and zeta potential

The mean particle size of the synthesized Se-NPs was determined to be approximately 56 nm, as observed in TEM micrographs (Fig. 7A). The nanoparticles fabricated under optimized synthesis conditions exhibited a zeta potential of -19.6 mV (Fig. 7B), indicating the presence of negatively charged functional groups on their surface. This negative surface charge contributes to colloidal stability through electrostatic repulsion; however, the magnitude of the zeta potential suggests moderate stability of nanoparticles in dispersion. Despite this, the Se-NPs remained well-dispersed without visible aggregation during storage and characterization. The moderate stability observed may be attributed not only to electrostatic interactions but also to steric hindrance provided by phytochemicals from *A. sativum* extract, which together help maintain nanoparticle dispersion in aqueous medium.

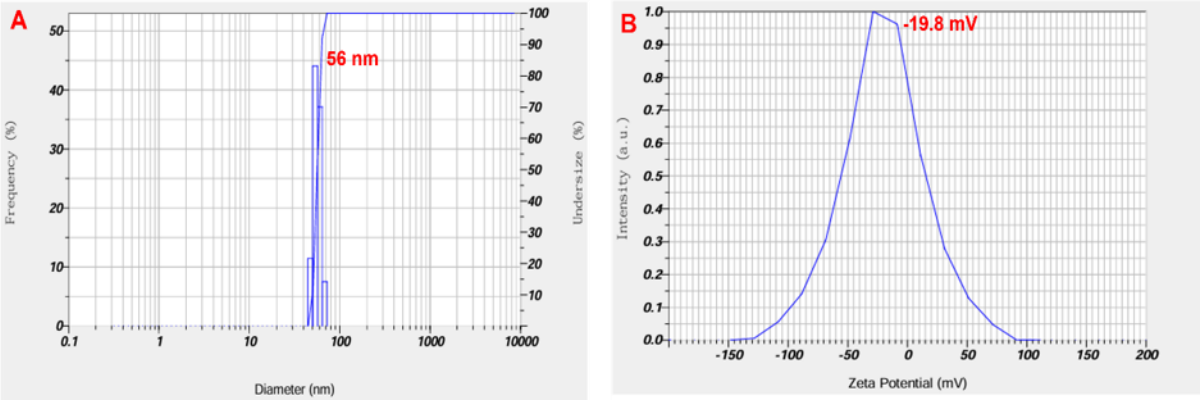


Fig. 7. (A) DLS and **(B)** Zeta potential of Se-NPs synthesized using *A. sativum* extract. Mean particle size ~56 nm; zeta potential –19.6 mV

Cell Viability

The MTT assay was utilized to assess the cytotoxicity of *A. sativum* extract and Se-NPs on MCF-7 cells. Growth inhibition percentages were determined relative to untreated control cells following treatment with escalating concentrations of the extract and Se-NPs (60, 120, and 240 µg/mL).

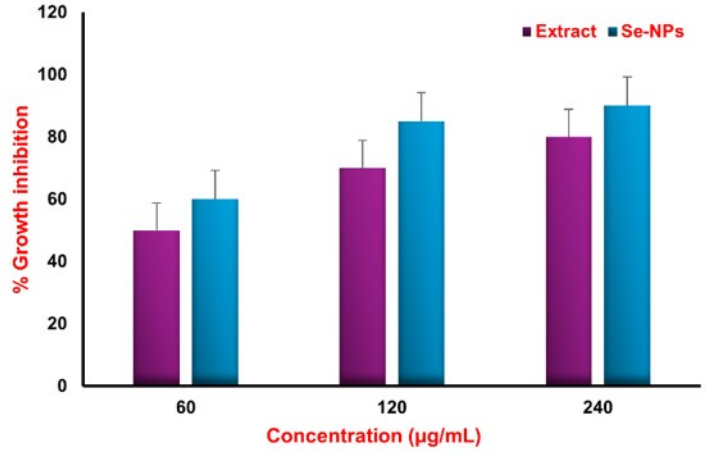


Fig. 8. Effect of Se-NPs and *A. sativum* extract on cell viability of MCF-7 and MCF-10A cells after 24 h

A pronounced concentration-dependent inhibition of MCF-7 cell growth was observed, as depicted in Fig. 8. The comparative IC_{50} values highlight distinct differences in cytotoxic potency among the tested treatments. The *A. sativum* extract exhibited an IC_{50} of ~165 µg/mL, reflecting moderate activity that is consistent with the presence of bioactive phytochemicals but insufficient for strong anticancer efficacy on its own. In contrast, Se-NPs demonstrated a lower IC_{50} of ~125 µg/mL, confirming enhanced cytotoxicity relative to the plant extract. These findings highlight that higher dose of Se-NPs significantly suppressed cancer cell proliferation, emphasizing their potential as effective anticancer agents.

Live-dead Assay

The AO/EB fluorescence staining assay was implemented to investigate the morphological modifications that are linked to apoptosis in MCF-7 cells. The distinct differentiation between viable and apoptotic cells is facilitated by this dual-staining method. Untreated control cells maintained their structural integrity and exhibited uniform green fluorescence, as illustrated in Fig. 9. This suggests that the cells were healthy and fully viable. On the other hand, cells that were exposed to the *A. sativum* extract and Se-NPs for 24 h exhibited distinct morphological characteristics of apoptosis. Orange to red fluorescence was observed in the stained apoptotic cells, indicating that the membrane integrity had been compromised. Membrane blebbing, nuclear fragmentation, and cell atrophy were prominently observed in the treated groups, which are additional hallmark features of apoptosis. These findings verify that apoptosis is induced in MCF-7 cells by both Se-NPs and the *A. sativum* extract in a dose-dependent manner.

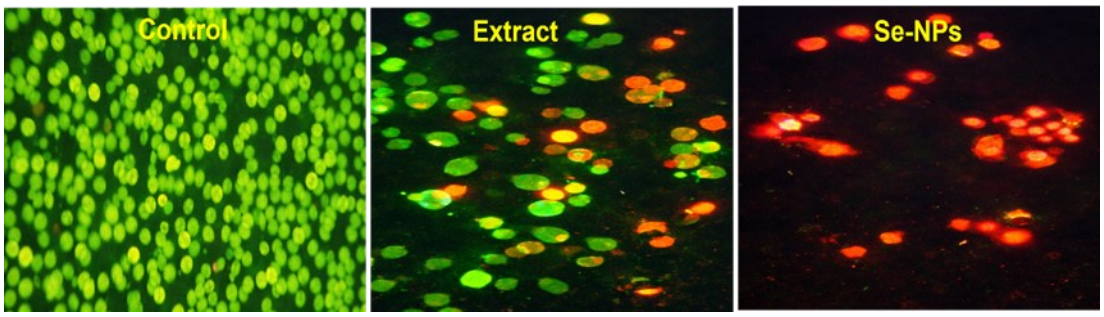


Fig. 9. AO/EB fluorescence staining of MCF-7 cells. Control cells showed intact morphology with green fluorescence, while treatment with *A. sativum* extract and Se-NPs induced orange-red fluorescence and apoptotic features, confirming dose-dependent cell death

Determination of ROS

The DCFH-DA assay was employed to quantify intracellular ROS generation to examine the influence of Se-NPs on oxidative stress. This method is predicated on the intracellular peroxide-dependent oxidation of non-fluorescent DCFH-DA to fluorescent DCF. The DCF fluorescence intensity of cells treated with Se-NPs for 24 h was significantly increased, suggesting that the ROS levels were elevated. Se-NPs substantially contribute to oxidative stress within cells, as evidenced by a significant increase in ROS levels in Se-NPs treated cells compared to the untreated control group (Fig. 10). Quantitative analysis confirmed this. The mechanism of apoptosis is widely acknowledged to be mediated by ROS generation, and the elevated ROS levels observed in Se-NPs treated cells are consistent with this.

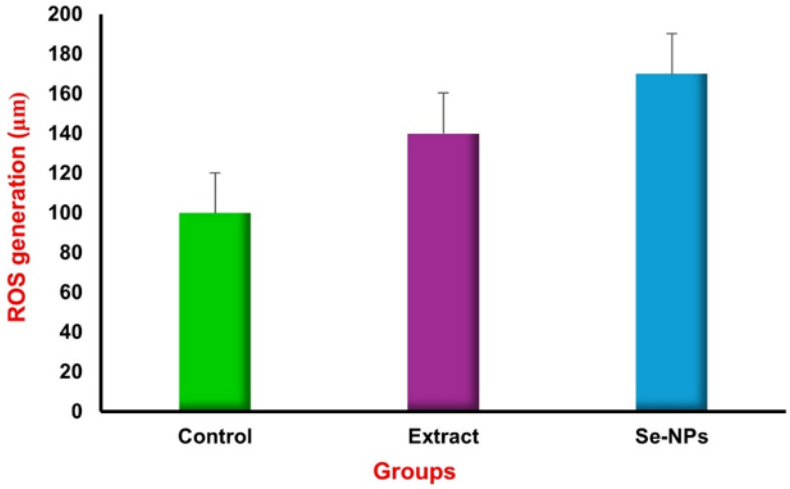


Fig. 10. Effect of Se-NPs on ROS generation in MCF-7 cells. Se-NPs significantly elevate ROS levels in a dose-dependent manner compared to controls

Caspase-3 and Caspase-9 Activities

The activity levels of caspase-3 and caspase-9 in MCF-7 cells treated with Se-NPs and *A. sativum* extract were compared to those of untreated controls to further validate apoptosis induction. Caspase-3 and caspase-9 are essential executors of the intrinsic apoptotic pathway, where they play critical roles in the terminal phase of programmed cell death when internal or external stimuli are activated. Treatment with Se-NPs and extract resulted in a twofold increase in the activities of both caspase-3 and caspase-9 in comparison to the control group, as illustrated in Fig. 11. This increased caspase activity indicates that Se-NPs effectively initiated apoptosis through mitochondrial signaling pathways. Furthermore, Se-NPs exposure is recognized to induce the production of ROS, which are responsible for DNA damage, endoplasmic reticulum stress, protein misfolding, and, in the end, apoptosis (Fig. 12). Upon activation, caspase-3 cleaves and activates caspase-activated DNase, which subsequently translocate to the nucleus and facilitates DNA fragmentation. This fragmentation, which is characterized by endonuclease activity, is widely acknowledged as a sign of early-stage apoptosis (Rafei *et al*. 2013).

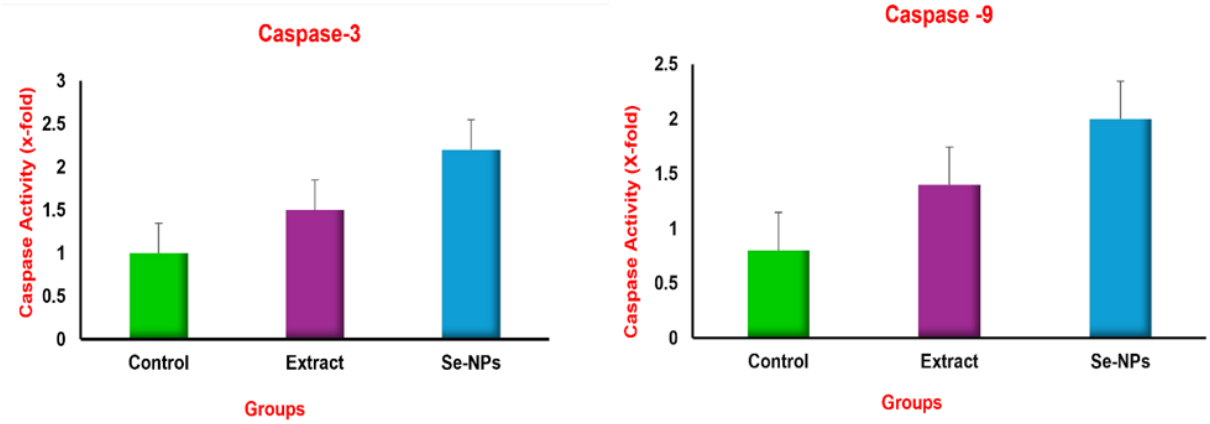


Fig. 11. Effect of Se-NPs on caspase-3 and caspase-9 activity in MCF-7 cells. Se-NPs increase caspase activity twofold, confirming ROS-mediated apoptosis induction.

To further clarify the mechanism of apoptosis, the activities of caspase-3 and caspase-9 were assessed in MCF-7 cells following Se-NP treatment. Both caspases exhibited approximately a twofold increase in activity relative to controls (Fig. 11). Caspase-9, an initiator of the intrinsic mitochondrial pathway, was activated in response to ROS-induced mitochondrial dysfunction, subsequently triggering caspase-3, the executioner caspase. Caspase-3 activation led to DNA fragmentation, a hallmark of programmed cell death. These findings establish that Se-NPs induce apoptosis through ROS-mediated mitochondrial signaling and caspase activation, thereby providing a mechanistic explanation consistent with the elevated ROS levels observed (Fig. 12).

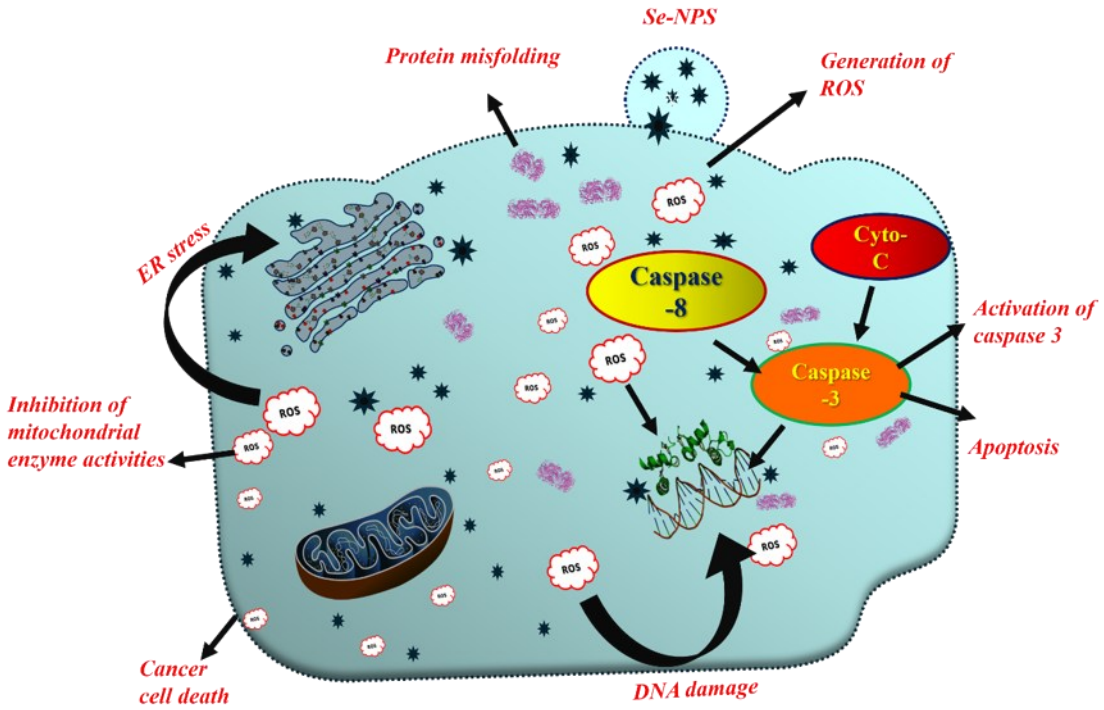


Fig. 12. The schematic illustrates the ROS-mediated mitochondrial pathway as the central mechanism underlying Se-NP-induced apoptosis.

CONCLUSION

1. Selenium nanoparticles (Se-NPs) were successfully synthesized using *Allium sativum* extract, with a mean size of ~56 nm, as confirmed by UV–Vis, transmission electron microscopy (TEM), and dynamic light scattering (DLS) analyses. The characteristic SPR peak at 280 nm validated nanoparticle formation, while TEM and DLS revealed uniform, monodisperse particles within the 40 to 100 nm range. Functionality was further supported by FTIR, X-ray diffraction (XRD), selected area electron diffraction (SAED), and energy-dispersive X-ray (EDX) analyses, confirming structural integrity and elemental composition.
2. Biological assays demonstrated that Se-NPs significantly elevated intracellular reactive oxygen species (ROS) levels, which in turn activated caspase-3 and caspase-9, leading to apoptosis in MCF-7 cells. Compared to the crude *A. sativum* extract, Se-NPs exhibited enhanced cytotoxicity with a lower IC_{50} value, underscoring their superior

anticancer potential. The findings highlight that *A. sativum*-mediated Se-NPs induce dose-dependent cytotoxicity through ROS generation and caspase activation.

3. Overall, these findings highlight the potential of *A. sativum*-mediated Se-NPs as promising applications in targeted breast cancer therapy. However, further mechanistic studies and in vivo validation are required before definitive therapeutic claims can be made.

ACKNOWLEDGEMENTS

Conflict of Interest

Authors have declared that no conflict of interest is associated with this work.

Data availability

The data associated with the findings of this study are available from the corresponding authors, upon reasonable request.

Funding

Authors have declared that no funding was associated with this work.

REFERENCES CITED

Alsammarraie, F. K., Wang, W., Zhou, P., Mustapha, A., and Lin, M. (2018). "Green synthesis of silver nanoparticles using turmeric extracts and investigation of their antibacterial activities," *Colloids and Surfaces B: Biointerfaces* 171, 398-405. https://doi.org/10.1016/j.colsurfb.2018.07.059

Alyamkina, E. A., Nikolin, V. P., Popova, N. A., Dolgova, E. V., Proskurina, A. S., Orishchenko, K. E., Efremov, Y. R., Chernykh, E. R., Ostanin, A. A., Sidorov, S. V., *et al*. (2010). "A strategy of tumor treatment in mice with doxorubicin-cy clophosphamide combination based on dendritic cell activation by human double stranded DNA preparation," *Genet. Vaccines Ther*. 8(1) -7. https://doi.org/10.1186/1479-0556-8-7

Azimizonuzi, H., Ghayourvahdat, A., Ahmed, M. H., Kareem, R. A., Zrzor, A. J., Mansoor, A. S., Athab, Z. H., and Kalavi, S. (2025). "A state-of-the-art review of the recent advances of theranostic liposome hybrid nanoparticles in cancer treatment and diagnosis," *Cancer Cell International* 25(1), 26. https://doi.org/10.1186/s12935-024-03610-z

Da-Yong, L., Ting-Ren, L., and Cao, S. (2013). "Drug combinations in cancer treatments," *Clin. Exp. Pharmacol.* 3, 1-8. https://doi.org/10.4172/2161-1459.1000134

Dennis, P. (2021). "Carnitine: its role in preventive medicine," *American Journal of Preventive Medicine and Public Health* 7, 1.

Forootanfar, H., Adeli-Sardou, M., Nikkhoo, M., Mehrabani, M., Amir-Heidari, B., Shahverdi, A. R., and Shakibaie, M. (2014). "Antioxidant and cytotoxic effect of biologically synthesized selenium nanoparticles in comparison to selenium dioxide," *Journal of Trace Elements in Medicine and Biology: Organ of the Society*

for Minerals and Trace Elements (GMS) 28(1), 75-79. https://doi.org/10.1016/j.jtemb.2013.07.005

Gupta, N., and Porter, T. D. (2001). "Garlic and garlic-derived compounds inhibit human squalene monooxygenase," *The Journal of Nutrition* 131(6), 1662-1667. https://doi.org/10.1093/jn/131.6.1662

Husen, A., and Siddiqi, K.S. (2014). "Plants and microbes assisted selenium nanoparticles: Characterization and application," *J. Nanobiotechnol.* 12, 28. https://doi.org/10.1186/s12951-014-0028-6

Iranifam, M., Fathinia, M., Sadeghi, T., Hanifehpour, Y., Khataee, A. R., and Joo, S. W., (2013). "A novel selenium nanoparticles-enhanced chemiluminescence system for determination of dinitrobutylphenol," *Talanta* 107, 263-269. https://doi.org/10.1016/j.talanta.2012.12.043

Kasibhatla, S., Amarante-Mendes, G. P., Finucane, D., Brunner, T., Bossy-Wetzel, E., and Green, D. R. (2006). "Acridine orange/ethidium bromide (AO/EB) staining to detect apoptosis," *CSH Protocols* 3, article 4493. https://doi.org/10.1101/pdb.prot4493

Kotepui, M. (2016). "Diet and risk of breast cancer," *Contemporary Oncology (Poznan, Poland)* 20(1), 13-19. https://doi.org/10.5114/wo.2014.40560

Leong, S. P., Shen, Z. Z., Liu, T. J., Agarwal, G., Tajima, T., Paik, N. S., Sandelin, K., Derossis, A., Cody, H., and Foulkes, W. D. (2010). "Is breast cancer the same disease in Asian and Western countries," *World Journal of Surgery* 34(10), 2308-2324. https://doi.org/10.1007/s00268-010-0683-1

Li S. K., Shen Y. H., Xie A. J., Xuerong, Q., Linguang, Z., and Li, Q., (2007). "Rapid, room-temperature synthesis of amorphous selenium/protein composites using *Capsicum annuum L* extract," *Nanotechnology* 18, article 405101. https://doi.org/10.1088/0957-4484/18/40/405101

Liu, C. T., Sheen, L. Y., and Lii, C. K. (2007). "Does garlic have a role as an antidiabetic agent," *Molecular Nutrition and Food Research* 51, 1353-1364. https://doi.org/10.1002/mnfr.200700082

Ma, X., Tian, Y., Yang, R. *et al.* (2024). "Nanotechnology in healthcare, and its safety and environmental risks," *J. Nanobiotechnol.* 22, article 715 (2024). https://doi.org/10.1186/s12951-024-02901-x

Müller, R. H., Mäder, K., and Gohla, S. (2000). "Solid lipid nanoparticles (SLN) for controlled drug delivery - A review of the state of the art," *European Journal of Pharmaceutics and Biopharmaceutics* 50(1), 161-177. https://doi.org/10.1016/s0939-6411(00)00087-4

Nwokocha, C. R., Ozolua, R. I., Owu, D. U., Nwokocha, M. I., and Ugwu, A. C. (2011). "Antihypertensive properties of *Allium sativum* (garlic) on normotensive and two kidney one clip hypertensive rats," *Nigerian Journal of Physiological Sciences: Official Publication of the Physiological Society of Nigeria* 26(2), 213-218. PMID: 22547193

Park, J. H., Lee, S., Kim, J. H., Park, K., Kim, K. and Kwon, I. C. (2008). "Polymeric nanomedicine for cancer therapy," *Progress in Polymer Science* 33, 113-137. http://dx.doi.org/10.1016/j.progpolymsci.2007.09.003

Patil, M. P., and Kim, G. D. (2018). "Marine microorganisms for synthesis of metallic nanoparticles and their biomedical applications," *Colloids Surfaces B Biointerfaces* 172, 487-495. https://doi.org/10.1016/j.colsurfb.2018.09.007

Prasad, K. S., and Selvaraj, K. (2014) "Biogenic synthesis of selenium nanoparticles and their effect on As(III)-induced toxicity on human lymphocytes," *Biol. Trace Elem. Res.* 157, 275-283. https://doi.org/10.1007/s12011-014-9891-0

Qi, R., Liao, F., Inoue, K., Yatomi, Y., Sato, K., and Ozaki, Y. (2000). "Inhibition by diallyl trisulfide, a garlic component, of intracellular Ca^{2+} mobilization without affecting inositol-1,4, 5-trisphosphate (IP(3)) formation in activated platelets," *Biochemical Pharmacology* 60(10), 1475-1483. https://doi.org/10.1016/s0006-2952(00)00467-6

Rafei, M., Dumont-Lagacé, M., Rouette, A., and Perreault, C. (2013). "Interleukin-21 accelerates thymic recovery from glucocorticoïd-induced atrophy," *PLoS ONE* 8(9), article e72801. https://doi.org/10.1371/journal.pone.0072801

Ramamurthy, C.h., Sampath, K. S., Arunkumar, P., Kumar, M. S., Sujatha, V., Premkumar, K., and Thirunavukkarasu, C. (2013). "Green synthesis and characterization of selenium nanoparticles and its augmented cytotoxicity with doxorubicin on cancer cells," *Bioprocess and Biosystems Engineering* 36(8), 1131-1139. https://doi.org/10.1007/s00449-012-0867-1

Shakibaie, M., Khorramizadeh, M. R., Faramarzi, M. A., Sabzevari, O., and Shahverdi, A. R. (2010). "Biosynthesis and recovery of selenium nanoparticles and the effects on matrix metalloproteinase-2 expression," *Biotechnology and Applied Biochemistry* 56(1), 7-15. https://doi.org/10.1042/BA20100042

Sharma, G., Sharma, A. R., Bhavesh, R., Park, J., Ganbold, B., Nam, J.-S., and Lee, S.-S. (2014). "Biomolecule-mediated synthesis of selenium nanoparticles using dried *Vitis vinifera* (Raisin) extract," *Molecules* 19(3), 2761-2770. https://doi.org/10.3390/molecules19032761

Shedbalkar, U., Singh, R., Wadhwani, S., Gaidhani, S., and Chopade, B. A. (2014). "Microbial synthesis of gold nanoparticles: Current status and future prospects," *Advances in Colloid and Interface Science* 209, 40-48. https://doi.org/10.1016/j.cis.2013.12.011

Shehata, N. S., Elwakil, B. H., Elshewemi, S. S. *et al.* (2023). "Selenium nanoparticles coated bacterial polysaccharide with potent antimicrobial and anti-lung cancer activities," *Sci Rep* 13, article 21871. https://doi.org/10.1038/s41598-023-48921-9

Shim, H. Y., Park, J. H., Paik, H. D., Nah, S. Y., Kim, D. S., and Han, Y. S. (2007). "Acacetin-induced apoptosis of human breast cancer MCF-7 cells involves caspase cascade, mitochondria-mediated death signaling and SAPK/JNK1/2-c-Jun activation," *Molecules and Cells 24*(1), 95-104. PMID: 17846503

Singh, R., Shedbalkar, U. U., Wadhwani, S. A. *et al.* (2015). "Bacteriagenic silver nanoparticles: Synthesis, mechanism, and applications," *Appl. Microbiol. Biotechnol.* 99, 4579-4593 https://doi.org/10.1007/s00253-015-6622-1

Srivastava, N., and Mukhopadhyay. M. (2015). "Green synthesis and structural characterization of selenium nanoparticles and assessment of their antimicrobial property," *Bioprocess and Biosystems Engineering* 38 (9), 1723-1730. DOI: 10.1007/s00449-015-1413-8.

Stockert, J. C., Blázquez-Castro, A., Cañete, M., Horobin, R. W., and Villanueva, A. (2012). "MTT assay for cell viability: Intracellular localization of the formazan product is in lipid droplets," *Acta Histochemica* 114(8), 785-796. https://doi.org/10.1016/j.acthis.2012.01.006

Tsubura A., Lai Y. C., Kuwata M., Uehara N., and Yoshizawa K. (2011). "Anticancer effects of garlic and garlic-derived compounds for breast cancer control," *Anticancer Agents Med. Chem*. 11(3), 249-253. https://doi.org/10.12691/jcrt-5-2-2

Vinaykumar, K., Kumar, V., and Stanley, L. (2003). *Robbins Basic Pathology*, 7 (Saunders, Philadelphia), 841. https://doi.org/10.1016/s0377-1237(04)80179-5

Wadhwani, S. A., Shedbalkar, U. U., Singh, R., and Chopade, B. A. (2016). "Biogenic selenium nanoparticles: current status and future prospects." *Applied Microbiology and Biotechnology* 100(6), 2555-2566. https://doi.org/10.1007/s00253-016-7300-7

Article submitted: February 21, 2026; Peer review competed: Mauy 31, 2026; Revised version received and accepted: June 23, 2026; Published: July 10, 2026.
DOI: 10.15376/biores.21.3.8015-8030